Insights into tunnelling rays: outperforming guided rays in fiber-optic sensing device

Jianjun Ma,[1,*] Wojtek J. Bock,[1] and Andrea Cusano[2]

[1]*Centre de recherche en photonique, Département d'informatique et d'ingénierie, Université du Québec en Outaouais, P.O. Box 1250, Station B, Gatineau, Québec J8X 3X7, Canada*
[2]*Optoelectronic Division, Engineering Department, University of Sannio, Benevento, Italy*
[*]*Corresponding author: ma.jianjun@uqo.ca*

Abstract: We report that, for an evanescent-wave (EW) based fiber-optic sensor, the less skewed tunnelling rays and a small number of very steep guided rays experience total internal reflection (TIR) at one end-face of the air-clad fiber segment. As a result, they demonstrate nine times greater efficiency in collecting EW-power than rays that do not exhibit end-face-TIR. This tunneling ray group originates from a launching ring that is seven times wider than that of end-face-TIR capable guided rays, enabling it to dominate the overall detected EW-power level. Strongly supporting this conclusion is the counter-intuitive experimental observation that the detected power at one end of the fiber abruptly drops 91% when the back reflection at the opposite end is eliminated, while an isotropic light source is placed at the core-cladding interface between these two ends. The mechanism of non-propagating ray excitation accounts for this high efficiency. We also indicate that many highly skewed tunnelling rays are naturally isolated from the external world because, outside the fiber core, they are accessible only via their EW fields even at the fiber end-faces. The findings reported here have significant implications for the design of future high-performance EW-based fiber sensing devices for the analysis of surface-event.

OCIS codes: (060.2370) Fiber Optics Sensors; (300.6280) Spectroscopy, fluorescence and luminescence; (060.2270) Fiber characterization.

References and links

1. A. W. Snyder, "Leaky-ray theory of optical waveguides of circular cross-section," Appl. Phys. **4**, 273-298 (1974).
2. A. W. Snyder and J. D. Love, *Optical Waveguide Theory* (Chapman and Hall Ltd., London, 1983).
3. Y. Xu, N. B. Jones, and J. C. Fothergill, "Theoretical analysis of the evanescent-wave absorption coefficient for multimode fiber-optic evanescent-wave absorption sensors," J. Mod. Opt. **46**, 2007-2014 (1999).
4. N. Issa, "High Numerical Aperture in Multimode Microstructured Optical Fibers," Appl. Opt. **43,** 6191-6197 (2004).
5. M. Åslund, S. D. Jackson, J. Canning, A. Teixeira, and K. Lyytikäinen-Digweed, "The influence of skew rays on angular losses in air-clad fibers," Opt. Commun. **262**, 77-81 (2006).
6. L. Poladian, N. Issa, and T. Monro, "Fourier decomposition algorithm for leaky rays of fibers with arbitrary geometry," Opt. Express **10**, 449-454 (2002). http://www.opticsinfobase.org/oe/abstract.cfm?URI=oe-10-10-449
7. Z. Zhang, Y. Shi, B. Bian, and J. Lu, "Dependence of leaky ray coupling on loss in photonic crystal fiber with hybrid cladding," Opt. Express **16**, 1915-1922 (2008). http://www.opticsinfobase.org/oe/abstract.cfm?URI=oe-16-3-1915
8. J. C. Flanagan, R. Amezcua, F. Poletti, J. R. Hayes, N. G. R. Broderick, and D. J. Richardson, "The effect of periodicity on the defect rays of large ray area microstructured fibers," Opt. Express **16**, 18631-18645 (2008). http://www.opticsinfobase.org/oe/abstract.cfm?URI=oe-16-23-18631
9. N. Issa and W. Padden, "Light acceptance properties of multimode microstructured optical fibers: Impact of multiple layers," Opt. Express **12**, 3224-3235 (2004). http://www.opticsinfobase.org/oe/abstract.cfm?URI=oe-12-14-3224

#108575 - $15.00 USD Received 12 Mar 2009; revised 17 Apr 2009; accepted 21 Apr 2009; published 23 Apr 2009

10. J. Ma and W. J. Bock, "Dramatic performance enhancement of evanescent-wave multimode fiber fluorometer using non-Lambertian light diffuser," Opt. Express **15**, 16457-16470 (2007). http://www.opticsinfobase.org/abstract.cfm?URI=oe-15-25-16457.
11. T. Yoshimura and Y. Koyamada, "Influence of tunnelling rays to baseband frequency response of step-index plastic optical fibers," Electron. Commun. Jpn. **88**, 12-17 (2005).
12. C. R. Taitt, T. P. Anderson, and F. S. Ligler, "Evanescent-wave fluorescence biosensors," Biosens. Bioelectron. **20**, 2470-2487 (2005).
13. J. Ma and W. J. Bock, "Reshaping sample fluid droplet: Towards combined performance enhancement of evanescent-wave fiber-optic fluorometer," Opt. Lett. **32**, 8-10 (2007).
14. G. Keiser, *Optical Fiber Communications* (McGraw-Hill Higher Education, third edition, 2000), Chap. 5.
15. P. DiVita and U. Rossi, "Realistic evaluation of coupling loss between different optical fibers," J. Opt. Commun. **1**, 26-32 (1980).
16. P. DiVita and U. Rossi, "Evaluation of splice losses induced by mismatch in fiber parameters," Opt. Quantum Electron. **13**, 91-94 (1981).

1. Introduction

Tunnelling rays, or leaky rays, feature extremely low loss even after traveling a long distance and in fact can be treated as guided rays [1, 2]. Research on tunnelling rays in the context of the conventional fiber framework is much less active today than it was two decades ago. Although related articles have continued to appear [3-9], most of them focus on the microstructured fibers which have become available in recent years, represented by Refs. [4-9]. Microstructured fibers feature numerous air holes surrounding a solid or hollow core to enable the index- or bandgap-based waveguide operation. The flexible combination of the number, size, shape and distribution of these holes provides virtually unlimited design variations and unusual characteristics that are not offered by conventional fibers. It is this reason that they have attracted so much attention. However, these air holes actually constitute a severe handicap when it comes to fabricating a real device. Contamination that may occur at the fiber end-face and the disappearance of air holes during the splicing of fibers are potential sources of problems for both device performance and the packaging process. These drawbacks, plus the more complex manufacturing process required, add significant extra costs as well as technical difficulties that do not exist when conventional fibers are used. In the foreseeable future, conventional fibers can be expected to continue to dominate the market and offer cost-effective solutions for a wide variety of fiber-optic devices. The enhancement of their performance by further extrapolation of existing theories is still an important objective. For example, tunnelling rays, which is generally regarded as a negative influence on fiber-optic communication systems [2, 11], may need to be re-evaluated with a view to enhancing fiber-optic sensing device performance. To our knowledge, the positive effects that the tunnelling rays can have on a fiber device have received very little attention. The paucity of papers on this topic points to a lack of direct experimental support [3] or to a need for further evidence to clarify how this ray category can contribute to overall device performance [3, 10].

Based on an in-depth investigation of the contribution of tunnelling rays to the overall power detected at the fiber end, this article will explore the remarkable impact they have on evanescent-wave (EW) based fiber-optic sensing performance. We will also establish that, in terms of wave-optics, when both tunneling and higher-order guided modes are present, the higher-order guided modes collect much less EW-power from the cladding area of optical fibers than the tunnelling modes do.

2. Theoretical background

A well-accepted concept associated with EW-based multimode fiber sensors or devices is that the EW-power arises mainly from higher-order guided modes [12]. Theoretically this is because their mode fields are less confined, especially in the case of modes near cutoff. In other words, higher percentages of the electric fields (in the form of EWs) of these modes appear at the cladding side of the core-cladding interface, allowing more efficient transfer of signal power from a sample located at this interface to the fiber core and thus to the detector at the fiber end. This concept, however, does not take into account the contribution of another

#108575 - $15.00 USD Received 12 Mar 2009; revised 17 Apr 2009; accepted 21 Apr 2009; published 23 Apr 2009

important mode category: tunnelling modes, or tunnelling rays in terms of ray-optics. Later in this article, we show how the tunnelling ray group plays a more significant role in enhancing EW-power collection efficiency.

Our study begins with a step-profile fiber as illustrated in Fig. 1, which gives a general ray path valid for all rays propagating along the fiber. This ray path can be described by the spherical polar angles θ_z and θ_ϕ and the incident angle α. The rays that may contribute to the overall power detected at the fiber end can be categorized according to the angles θ_z and α by [2]:

Guided rays: $$0 < \theta_z < 90^\circ - \alpha_c \tag{1}$$

Tunnelling rays: $$90^\circ - \alpha_c < \theta_z < 90^\circ \quad \text{and} \quad \alpha_c < \alpha < 90^\circ \tag{2}$$

where α_c is the critical angle.

For the waveguide shown in Fig. 1, Eq. (1) describes both meridional guided rays and the longer-pitched helical, or skew-type guided rays, while Eq. (2) shows that tunnelling rays are closely related to skew-type guided rays but follow helical paths that are even shorter pitched. The shortest pitch is found when both $\theta_z \to 90^\circ$ and $\alpha \to 90^\circ$ are fulfilled. A particularly interesting example, as shown in Fig. 2, is a multimode fiber divided into several segments which are covered by surrounding materials with different refractive indices (RIs). To facilitate our analysis, we adopt the RIs of a specific multimode fiber used in our study, which involves a glass core covered by air, polymer and liquid claddings with RIs of $n_{co} = 1.46$, $n_{air} = 1$, $n_{pl} = 1.41$ and $n_{liq} = 1.33$. The critical angle of each individual segment is determined by $\alpha_c = \sin^{-1}(n_{cl}/n_{co})$. Obviously, we have $\alpha_{c\_air} < \alpha_{c\_liq} < \alpha_{c\_pl}$. The very steep guided rays, associated with very high-order guided modes, are those with incident angles close to α_{c_air} and possess the highest EW-power collection capability within the category of guided rays. The differences between the critical angles indicate the launching angles that are inhibited when the rays travel from the segment with a smaller α_c to the one with a larger α_c. This is especially our case since rays follow the path of air-clad segment → liquid-clad segment → polymer-clad segment. It is these blocked rays that are highly efficient in collecting EW power. Fortunately, our study presented later indicates that for a short fiber in the length of few meters, these rays are able to enter into the segment with polymer-clad via the excitation of non-propagating modes and thus affect the level of detectable EW-power to a significant degree.

A deeper examination of Fig. 1, Eqs. (1) and (2) shows that angle θ_z also represents the angle of incidence of the ray on the fiber end-face. We can see that, for a fiber core surrounded by air cladding, total internal reflection (TIR) from the fiber end-face will be experienced by the very steep guided rays launched from $43^\circ < \theta_z < 47^\circ$. Tunnelling rays can be divided into two groups. Those falling into $47^\circ < \theta_z < 75^\circ$ & $43^\circ < \alpha < 75^\circ$, belonging to the category of less skewed tunnelling rays, experience end-face-TIR within the air-clad fiber segment. Other tunnelling rays, launched from $75^\circ < \theta_z, \alpha < 90^\circ$, are allowed by all three fiber segments and may experience multiple back-and-forth loops of end-face-TIR between the S- and R-end faces. Although a brief mention of end-face-TIR based on wave-optics is found in [4] in reference to a microstructured fiber with a very large NA close to 1, our straightforward investigation based on ray-optics reveals more abundant information. We disclose not only the occurrence of end-face-TIR in conventional fiber with an NA as low as 0.37, but also the range of angles needed to launch the rays that are capable of end-face-TIR. We further

#108575 - $15.00 USD Received 12 Mar 2009; revised 17 Apr 2009; accepted 21 Apr 2009; published 23 Apr 2009

indicate that certain tunnelling rays undergo the repetitive end-face-TIR process at both fiber ends.

The concept of end-face-TIR is somewhat startling since common knowledge in the field of fiber optics holds that a fiber end-face allows most of the power to pass through rather than fully reflecting it. The concept can be clarified by a further calculation from Eqs. (1) and (2) which shows that end-face-TIR is limited to tunnelling and very steep guided rays. The majority of guided rays – well-guided rays associated with well-confined lower-order guided modes, including both meridional and skew types, have their incident angles outside the range $43^\circ < \theta_z < 47^\circ$ (or obeying $0 < \theta_z < 43^\circ$) and are not eligible for end-face-TIR.

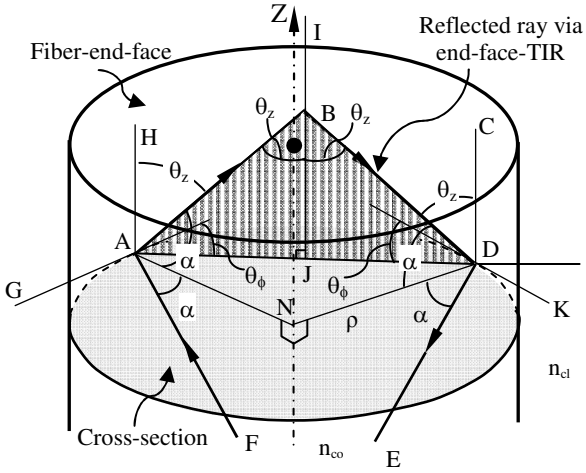

Fig. 1. A typical skew ray path within a step-profile fiber waveguide when end-face-TIR occurs. ρ : fiber core radius; α : incident and reflected angle; θ_z : angle of incident and reflected rays with fiber axial direction AH; θ_ϕ : the angle between the ray projection onto the fiber cross-section AD and the tangent AG.

3. Experimental verification

3.1 Design of experimental approach to highlight rays capable of end-face-TIR

Experimentally verifying the above theoretical findings requires a proper means to highlight those rays capable of end-face-TIR and to suppress others that are well-guided. Feeding excitation power from the fiber end-face to excite the sample, as is typically done in a traditional EW-based fiber-optic sensor, will inevitably couple a significant amount of power to the lower-order modes, introducing a high noise level into the detector and making it difficult to identify the power carried by targeted modes or rays.

A proper experimental approach depends on a thorough understanding of the characteristics of end-face-TIR rays. In terms of wave-optics, very high-order guided modes operate near cutoff, showing that their mode fields extend more deeply into the cladding than would be expected from other guided modes. Further, all tunnelling modes operate just below cutoff, suggesting an even higher scale of such penetration. It is thus expected that tunnelling modes possess the highest efficiency in collecting EW-power among all targeted modes. Our previously proposed single-sampling-channel evanescent-wave fluorescent sensor, designed to highlight EW fluorescent signal power and avoid lower-order mode excitation, is an ideal tool for this particular study [13]. As illustrated in Fig. 2, the receiving fiber (r-fiber), having an uncladded segment at one end for sensing purposes (S-end), is a step-profile multimode fiber with a core / cladding / jacket size of 400 / 430 / 730 μm as well as the NA of 0.37. The other end of the r-fiber (R-end) is directly connected to a spectrometer. The illuminating fiber

#108575 - $15.00 USD Received 12 Mar 2009; revised 17 Apr 2009; accepted 21 Apr 2009; published 23 Apr 2009

(i-fiber), pigtailed with a 3-mW laser diode operating at 532 nm, has core / cladding / jacket dimensions of 300 / 330 / 670 μm. By slightly moving the i-fiber to reshape a sample droplet, we achieve dramatically enhanced EW-power and eliminate stray excitation light, ensuring that only ray groups with a higher percentage of their associated mode fields in the cladding region will be highlighted, especially those near or just below cutoff. This design minimizes the excitation power level at the R-end since the laser launching angle created in this setup is nearly perpendicular to the fiber axis OZ in Fig. 2 and thus the excitation of any core modes is naturally inhibited.

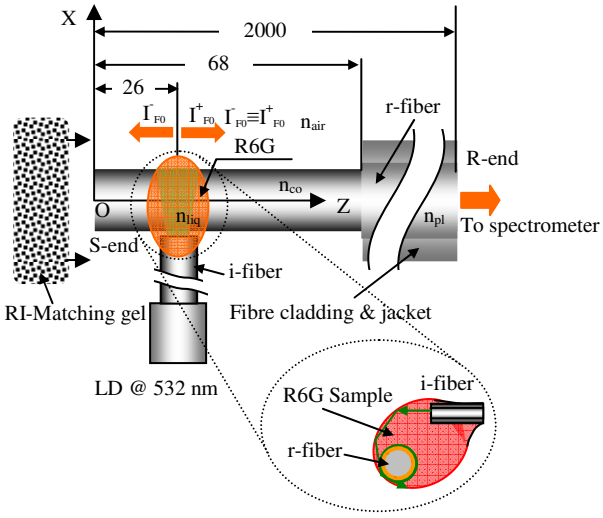

Fig. 2. EW-based fluorescent fiber-optic sensing setup for end-face-TIR demonstration. Inset: separation between the i- and r- fibers when the optimum power is achieved. Air-, liquid- (R6G sample) and polymer-cladding segments are identified by their corresponding RIs as marked. An RI-matching gel block is introduced to eliminate any reflections at the fiber end-face. Refer to [13] for more detailed description of the operation of this sensor.

3.2 Experimental verification and results

We now examine the power variations at the R-end by changing the RI of the immersion medium in front of the opposite end, the S-end. This RI variation is simply achieved by exposing the end-face at the S-end to air and to a large RI-matching gel block ϕ24×30 mm in size, respectively. The gel block has an RI matching that of the fiber core, and will therefore completely remove any back reflections, including TIR. We expect a very high drop in power after we eliminate TIR, which is required to prove the validity of our theoretical finding. As in Fig. 2, the S-end of a fiber approximately 2 meters in length is decladded to expose a 68 mm segment of the core to the surrounding air. A Rhodamine 6G (R6G) sample droplet described in [13] is dispensed at z = 26 mm. With the spectrometer connected to the R-end, we record the spectra before and after moving the gel block to z = 0 of the S-end.

Curves ① and ② in Fig. 3 reveal that the highest power level appears when the fiber end-face is exposed to air. Curve ② shows a dramatic drop in power of about 91% when the fiber end-face is in contact with the gel block, suggesting the cancellation of enormous reflection at this location. Although this is already strong evidence of the existence of end-face-TIR, one may argue that this power drop could be caused not by blocking TIR but merely by blocking a larger reflection. This possibility can be ruled out by referring to the Fresnel equations, according to which, for either *p* or *s* components, a dramatic drop in reflection ratio occurs to a ray with an incident angle even slightly below the critical angle at the core-air interface. For example, the critical angle at the core-air interface is $\alpha_c = 43.231^\circ$, and a 91% reflection ratio

#108575 - $15.00 USD Received 12 Mar 2009; revised 17 Apr 2009; accepted 21 Apr 2009; published 23 Apr 2009

requires an incident angle of $\theta_z = 43.215^\circ$ for *s* components and $\theta_z = 43.228^\circ$ for *p* components. At $\theta_z = 43^\circ$, the reflection ratio abruptly drops to 47% for *p* components and 70% for *s* components. With these calculations as additional evidence, the occurrence of end-face-TIR is now fully confirmed.

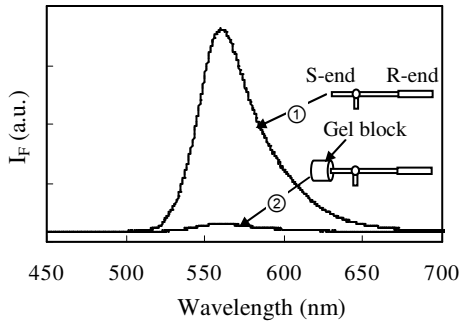

Fig. 3. Experimental evidence of the occurrence of end-face-TIR from observing EW-power variations when the S-end-face is exposed to a low- (air, $n_{air} = 1$) and a high-RI medium (RI-matching gel block ϕ24×30 mm, $n_{gel} = 1.465$). Curve ①: EW fluorescent spectrum when the S-end is exposed to the air medium; curve ②: EW fluorescent spectrum when the S-end is exposed to the gel block medium. The striking 91% power drop, apparently counter-intuitive, can only be interpreted as the elimination of end-face-TIR. Refer to the text for detail.

4. Further discussion

4.1 A counter-intuitive phenomenon

Now we begin to understand how this finding – the existence of the end-face-TIR process – leads to the observed but counter-intuitive phenomenon of a 91% drop in power by eliminating the back reflection at the opposite fiber end-face. The symmetrical architecture in Fig. 2 determines that the initial levels of EW-power I_{F0}^{+} and I_{F0}^{-}, traveling on the two sides of the R6G sample droplet in opposite directions (+z and -z), will be identical. We expect that EW-power I_{F0}^{+} will be dominant in the overall detected power. However, the cancellation of 91% of the power at z = 0 of the S-end suggests the contrary: a detector at the R-end was able to detect 91% of the I_{F0}^{-} power reflected from a mirror-like end-face at the S-end, but only 9% of the power I_{F0}^{+} (with $I_{F0}^{+} \equiv I_{F0}^{-}$) directly sent to it, although in both cases, the power originates from the same isotropic light source – the R6G sample. Moreover, by carefully examining the air-clad segment of the r-fiber in Fig. 2, we see further the apparent power anomalies: before merging with I_{F0}^{+} and propagating towards the R-end, power I_{F0}^{-} has to complete an additional loop trip of R6G → 26 mm fiber segment to the left → fiber end-face at z = 0 → TIR at z = 0 →26 mm fiber segment to the right → R6G sample → merging with I_{F0}^{+}.

4.2 Several significant conclusions

An obvious question arises: how does I_{F0}^{-} not only survive these extra travels but also deliver nine times more power to the R-end than I_{F0}^{+} does?

To answer this question, we need to clarify four central points by comparing Eq. (1) with the requirement of $\theta_z > 43.231^\circ$ for end-face-TIR as indicated in section 3.2 and the observation that 91% of the power is reflected back from the S-end.

#108575 - $15.00 USD Received 12 Mar 2009; revised 17 Apr 2009; accepted 21 Apr 2009; published 23 Apr 2009

First, 9% of the overall power is still detectable at the R-end after we cancel the back reflection at the S-end. In other words, this percentage reflects the amount of EW-power collected by the ray group that is incapable of end-face-TIR. This ray group includes almost all guided rays except for a small number of very steeply launched guided rays that are in fact capable of end-face-TIR and that are allowed in the air-clad fiber segment. This 9% of overall power is unaffected simply because this portion of power is directly sent to the R-end from the R6G sample via a one-way trip without experiencing end-face-TIR. Moreover, none of the guided rays propagating along the liquid- or polymer-clad fiber segments, whether meridional or skewed types, are capable of end-face-TIR.

Second, a group of highly-skewed tunnelling rays may experience multiple end-face-TIRs between the S- and R-ends and is allowed in all three segments (air-, liquid- and polymer-clad segments). These rays are excited from a large ring that obeys $75^\circ < \theta_z, \alpha < 90^\circ$.

Third, in terms of wave-optics, end-face-TIR tunnelling modes are highly efficient in collecting EW power, as discussed in section 3.1. These modes in fact receive more EW-power than would be expected from higher-order guided modes of either the meridional or the skew type.

Fourth, in the air-clad segment, light rays falling within a narrow ring of about 4° ($43^\circ < \theta_z < 47^\circ$) experience end-face-TIR only once. These rays have very steep incident angles and are associated with very high-order guided modes. Similarly, one-time end-face-TIR is also experienced by less-skewed tunnelling rays launched from $47^\circ < \theta_z < 75^\circ$ & $43^\circ < \alpha < 75^\circ$, and associated with an ring as wide as 28°.

4.3 Three groups of end-face-TIR capable rays: theoretical and experimental investigations

We now have three groups of rays capable of end-face-TIR which may contribute to the 91% level of overall EW-power received at the R-end: highly skewed tunnelling rays ($75^\circ < \theta_z, \alpha < 90^\circ$), very steep guided rays ($43^\circ < \theta_z < 47^\circ$), and less skewed tunnelling rays ($47^\circ < \theta_z < 75^\circ$ & $43^\circ < \alpha < 75^\circ$). Each group has to overcome its own specific obstacles in order to be received by the detector at the R-end.

1. Highly skewed tunnelling rays ($75^\circ < \theta_z, \alpha < 90^\circ$): as indicated before, this ray group is allowed by all three fiber segments and would seem to be a possible contributor to overall EW power. However, for this ray group, the end-face-TIR process takes place at not only the S-end but also the R-end. Multiple back-and-forth TIRs between the faces of the S- and R-ends may occur before all the power they carry is depleted for such reasons as their leaky nature and the associated mode coupling process. We expect that this ray group is undetectable, which can be confirmed from both theoretical and experimental respects. Theoretically, we consider that the mode coupling process which always exists in a defective waveguide may cause a power transfer to detectable rays. However, efficient mode coupling requires phase matching, a condition which may be satisfied by neighbouring modes associated with rays that travel at slightly different angles. This condition becomes mandatory when the waveguide is short and lacks any form of periodical modifications as in our case. We found that there is no overlap between this ray group ($75^\circ < \theta_z, \alpha < 90^\circ$) and its closest neighbor, the detectable less skewed tunnelling ray group ($15^\circ < \theta_z < 75^\circ$ & $75^\circ < \alpha < 90^\circ$). At this point, we conclude that very highly skewed tunnelling rays may not contribute to the overall detectable EW power.

Experimentally, we reverse the S- and R-ends of the fiber in Fig. 2 and record the variations of EW-power at the S-end by repeating the same experimental steps used for Fig. 3. A segment of large-core fiber with a core size of 800 μm is used to connect the R-end with the spectrometer. The idea of this experiment is that if the rays that are capable of back-and-forth end-face-TIR significantly affect the overall detectable power, we should be able to observe from the S-end a sharp drop in power similar to Fig. 3 by eliminating the back reflection at the

#108575 - $15.00 USD Received 12 Mar 2009; revised 17 Apr 2009; accepted 21 Apr 2009; published 23 Apr 2009

R-end. However, in direct contrast to Fig. 3, the results of this experiment, illustrated in Fig. 4, show nearly unchanged EW-power levels. This is remarkable experimental evidence further confirming that the very highly skewed tunnelling rays do not contribute to overall detected EW power.

2. Very steep guided rays (launched within a 4° ring) and less skewed tunnelling rays (launched within a 28° ring): As indicated before, at first sight it appears that both groups should be blocked when encountering either the liquid- or the polymer-clad fiber segment. However, research shows [14] that in the first few tens of meters of the fiber, non-propagating rays might be excited. In other words, our two-meter r-fiber allows these two ray groups to carry a significant amount of power into the polymer-clad segment and arrive at the R-end. Now we have both theoretical and experimental evidence to confirm that overall EW-power comes mainly from these two ray groups.

The process of excitation of non-propagating rays can be further used to elucidate the impact of extra loop travel of I_{F0}^{-} mentioned at the end of section 4.1 and the beginning of section 4.2: the looping path followed by power I_{F0}^{-} leads to an additional power scattering process on a remarkable scale. It is this extra process that dramatically increases the percentage of power I_{F0}^{-} detected at the R-end.

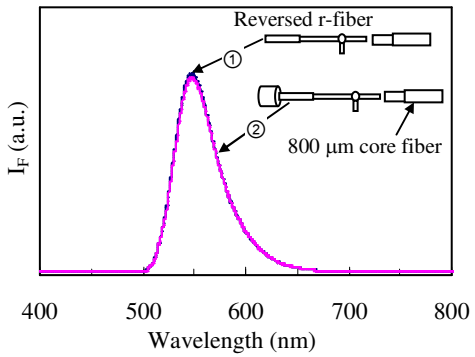

Fig. 4. Experimental results when the r-fiber in Fig. 2 is reversed and the experimental steps for Fig. 3 are repeated. A segment of large-core fiber with 800 μm core size is used between the spectrometer and the r-fiber to facilitate the connection. Curve ①: EW-power spectrum when the R-end is exposed to the air medium; curve ②: EW fluorescent power spectrum when the R-end is in contact with the gel block. The nearly unchanged EW fluorescent power level confirms that very highly skewed end-face-TIR tunnelling rays make no contribution to overall detectable EW-power.

4.4 Less skewed tunnelling rays: the major contributor of detectable EW-power

Another important fact revealed by our investigation is that the less skewed tunnelling rays are launched from a ring seven times wider than the launching ring of steep guided rays. As a result, this tunnelling ray group plays the major role in collecting EW-power and delivering it to the R-end.

4.5 Revisiting the mechanism for non-propagating ray excitation

As discussed in section 4.3, 91% of the detected EW-power stems from the non-propagating ray excitation process. This is similar to power coupling between two different fibers, but in our case, the air-clad segment acts as the source fiber while the polymer-clad segment serves as the receiving fiber. The precise calculation of coupling between these two fibers requires taking into account the non-uniform distribution of power among the rays (exactly the

#108575 - $15.00 USD Received 12 Mar 2009; revised 17 Apr 2009; accepted 21 Apr 2009; published 23 Apr 2009

situation in our study). Such an analysis has been reported in considerable detail in Refs [15, 16].

4.6 Deeper insight into the end-face-TIR capable rays

We now provide a deeper insight into the effects and behaviors of all three groups of rays that are capable of end-face-TIR.

The overall detectable EW-power at the R-end can be simulated by a simplified model of Fig. 2, which is illustrated in Fig. 5. Again, we have $I_{F0}^{+} \equiv I_{F0}^{-}$. The S- and R-ends have their reflection and transmission ratios as well as their transmitted power denoted as R_S, T_S, I_S and R_R, T_R, I_R, respectively. By assuming multiple internal reflections between the two fiber ends, the detected power at R-end can be written as:

$$\begin{aligned} I_R &= I_{F0}^{-}(R_S \times T_R + R_S R_R \times R_S T_R + R_S R_R R_S R_R \times R_S T_R + R_S R_R R_S R_R R_S R_R \times R_S T_R + \ldots) + \\ &\quad + I_{F0}^{+}(T_R + R_R \times R_S T_R + R_R R_S R_R \times R_S T_R + R_R R_S R_R R_S R_R \times R_S T_R + \ldots) \\ &= \frac{I_0}{2} T_R R_S (1 + R_S R_R + R_S^2 R_1^2 + R_S^3 R_R^3 + \ldots) + \frac{I_0}{2} T_R (1 + R_R R_S + R_R^2 R_S^2 + R_R^3 R_S^3 + \ldots) \\ &= \frac{I_0}{2} T_R (R_S + 1)[\frac{1 - (R_R R_S)^m}{1 - R_R R_S}] \\ &= \frac{I_0}{2} \frac{(1 - R_R)(1 + R_S)}{1 - R_R R_S} \quad \text{when} \quad m \to \infty \end{aligned} \tag{3}$$

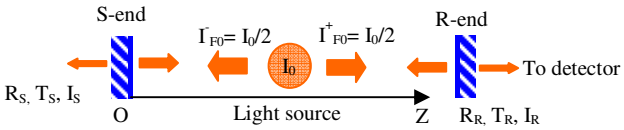

Fig. 5. Simplified model based on Fig. 2.

where m represents the number of reflections or transmissions at the S- or the R-end and may be a large value for rays capable of back-and-forth end-face-TIR. The following facts are used to derive Eq. (3): $T_R = 1 - R_R$, $R_S < 1$ and $R_R < 1$.

The percentage of EW-power received at the R-end I_R versus the overall power I_0 is:

$$\frac{I_R}{I_0} = \frac{0.5 \times (1 - R_R)(1 + R_S)}{(1 - R_R R_S)} \times 100\% \tag{4}$$

For the two detectable rays groups, Eq. (3) is still applicable when examining the deriving procedures of Eq. (3). Thus we can set $R_R \approx 0$ and obtain:

$$\frac{I_R}{I_0} = 0.5 \times (1 + R_S) \times 100\% \tag{5}$$

When the end-face-TIR occurs at the S-end, $R_S = 1$ and we find:

$$I_R = I_0 \tag{6}$$

Equation (6) states the fact that the overall detected power is the sum of I_{F0}^{+} and I_{F0}^{-}.

As a comparison, let us consider the case when the same percentage of reflection takes place at both the S- and the R-ends, that is $R_S = R_R$. Equation (4) then becomes:

#108575 - $15.00 USD Received 12 Mar 2009; revised 17 Apr 2009; accepted 21 Apr 2009; published 23 Apr 2009

$$I_R \equiv 0.5 I_0 \Big|_{R_S = R_R} \tag{7}$$

Equation (7) also applies to the very highly skewed tunnelling ray group with $R_S = R_R = 1$. Interestingly, the power level $I_R = 0.5 I_0$ carried by this ray group can also be achieved by removing both the S- and the R-end faces, or setting $R_S = R_R = 0$! This result indicates that, even presuming one can find a way to receive the power carried by this ray group at the R-end, it is still only half as efficient as the other two ray groups in sending collected EW-power to the R-end for detection.

5. Conclusions

The prime significance of this work lies in its revelation of the superior performance of tunnelling rays / modes in collecting detectable EW-power from a sample positioned at the cladding area.

The work is also significant because it shows that two separated groups of tunnelling rays have to be considered based on their substantially different behaviors in collecting and sending EW-power for detection. One group, highly skewed, may experience multiple end-face-TIRs between the two fiber ends and is undetectable without taking specific measures. The other group, less skewed, has a much wider launching ring and is far more efficient than very steep guided rays in collecting and sending detectable EW power. Moreover, the highly skewed end-face-TIR tunnelling rays can be excited only from the fiber end-face through their EW fields, implying that this ray category is isolated from interference by all external light sources beyond the EW-occupied surface layer, from either the curved side-wall surface or the end-faces.

The excitation of non-propagating rays, considered as a loss mechanism when a long fiber is involved, becomes beneficial for a short fiber and accounts for this enormous EW-power increase.

This study also reveals that the high collection efficiency reported here may be achieved without modifying the sensing segment to a specific shape such as a taper, as is often done in traditional EW-based fiber sensors [12]. The only requirement in our design is to expose the S-end to the surrounding air immersion medium. Our design offers an extremely cost-effective solution while dramatically enhancing EW-signal level. Furthermore, it uses a tiny droplet sample only few microliters in size and minimizes the noise from the excitation source, as discussed in our previous work [13]. This novel approach paves the way towards a new class of high performance EW-based fiber sensing device for the analysis of surface-event.

Acknowledgments

The authors gratefully acknowledge support for this project from the Natural Sciences and Engineering Research Council of Canada, from the Canada Research Chairs Programme and from le Ministère du Développement économique, de l'Innovation et de l'Exportation (MDEIE) du Québec.

#108575 - $15.00 USD Received 12 Mar 2009; revised 17 Apr 2009; accepted 21 Apr 2009; published 23 Apr 2009